

# A statistical model of elasto-plastic asperity contact between rough surfaces

Robert L. Jackson<sup>a,\*</sup>, Itzhak Green<sup>b</sup>

<sup>a</sup>*Department of Mechanical Engineering, Auburn University, Auburn, AL 36849-5341, USA*

<sup>b</sup>*George W. Woodruff School of Mechanical Engineering, Georgia Institute of Technology, Atlanta, GA 30332-0405, USA*

Received 17 September 2004; received in revised form 7 September 2005; accepted 19 September 2005

Available online 25 October 2005

## Abstract

This work models statistically elasto-plastic contact between two rough surfaces using the results of a previous finite element analysis of an elasto-plastic sphere in contact with a rigid flat. The individual asperity contact model used accounts for a varying geometrical hardness effect that has recently been documented in previous works (where geometrical hardness is defined as the uniform pressure found during fully plastic contact). The contact between real surfaces with known material and surface properties, such as the elastic modulus, yield strength, and roughness are modeled. The asperity is modeled as an elastic-perfectly plastic material. The model produces predictions for contact area, contact force, and surface separation. The results of this model are compared to other existing models of asperity contact. Agreement exists in some cases and in other cases it corrects flaws, especially at large deformations. The model developed by Chang, Etsion and Bogy is also shown to have serious flaws when compared to the others. This work also identifies significant limitations of the statistical models (including that of Greenwood and Williamson).

© 2005 Elsevier Ltd. All rights reserved.

*Keywords:* Rough surface; Contact mechanics; Elasto-plastic

## 1. Introduction

Since in reality all engineering surfaces are rough to some degree, the modeling of the contact between these rough surfaces is very important. Modeling the contact between rough surfaces leads to an improved understanding of the friction, wear, and thermal and electrical conductance between surfaces. When loading presses two rough surfaces together, only the peaks or asperities on the surface will be in contact. Thus, the asperities or peaks of the surfaces often carry very high loads. These high loads will often cause yielding in the surface material and thus purely elastic contact models of rough surfaces are not always adequate.

One of the earliest models of elastic asperity contact is that of Greenwood and Williamson (GW) [1]. This GW

model uses the solution of the contact of an elastic hemisphere and a rigid flat plane, otherwise known as the Hertzian solution, to stochastically model an entire contacting surface of asperities with a postulated Gaussian height distribution. The GW model also assumes that the asperities do not interfere with adjacent asperities and that the bulk material below the asperities does not deform. Supplementing the GW model, many elasto-plastic asperity models have been devised. Appendix A provides a summary of these models. Although these previous models have proven useful, they contain clear pitfalls which may be detrimental to their validity as described in Appendix A. The following work attempts to provide a more accurate model and also a clearer understanding of its and its predecessors' limitations.

As the load or interference increases, the stresses within the hemisphere also increase. These stresses eventually cause the material within the hemisphere to yield. The interference at this initial point of yielding is known as the critical interference,  $\omega_c$ . The recent work by Jackson and

\*Corresponding author.

*E-mail addresses:* [robert.jackson@eng.auburn.edu](mailto:robert.jackson@eng.auburn.edu) (R.L. Jackson), [itzhak.green@me.gatech.edu](mailto:itzhak.green@me.gatech.edu) (I. Green).



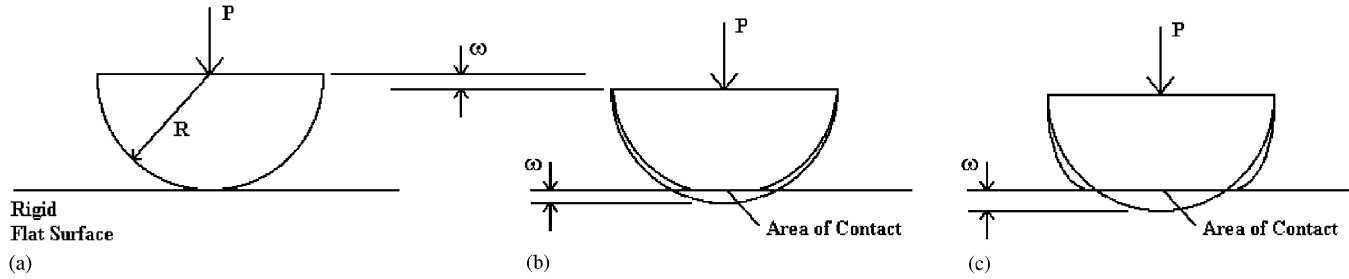


Fig. 1. Spherical contact model before contact (a), during mostly elastic deformation (b), and during mostly plastic deformation (c).

$$\bar{P}_{JG} = \bar{P}_c \left\{ \left[ \exp \left( -\frac{1}{4} \left( \frac{\omega}{\omega_c} \right)^{5/12} \right) \right] \left( \frac{\omega}{\omega_c} \right)^{3/2} + \frac{4H_G}{CS_y} \left[ 1 - \exp \left( -\frac{1}{25} \left( \frac{\omega}{\omega_c} \right)^{5/9} \right) \right] \frac{\omega}{\omega_c} \right\}, \quad (6)$$

where

$$B = 0.14 \exp(23e_y), \quad (7)$$

$$e_y = \frac{S_y}{E'}, \quad (8)$$

$$\frac{H_G}{S_y} = 2.84 \left[ 1 - \exp \left( -0.82 \left( \sqrt{\frac{\omega}{R}} \left( \frac{\omega}{1.9\omega_c} \right)^{B/2} \right)^{-0.7} \right) \right]. \quad (9)$$

Eq. (9) describes the varying geometric hardness of a hemispherical asperity in flattening defined in [2], which is different than the commonly defined indentation hardness [5].

Statistically, Eq. (5) differs from FEM data by an average of 1.3% and a maximum of 4.3%. While Eq. (6) differs by an average error of 0.94% and a maximum of 3.5%. Quicksall et al. [6] also confirmed these results for a wider range of materials by varying  $E$ ,  $S_y$  and  $v$ .

### 3. Statistical model

This work uses a Gaussian distribution for the asperity height distribution that is given as

$$\phi = \frac{(2\pi)^{-1/2}}{\sigma_s} \exp \left[ -0.5 \left( \frac{z}{\sigma_s} \right)^2 \right], \quad (10)$$

where  $\sigma_s$  is the standard deviation of the asperity heights. McCool [7] has related these values to the overall roughness of the surface as follows:

$$\sigma^2 = \sigma_s^2 + \frac{3.717 \times 10^{-4}}{\eta^2 R^2}, \quad (11)$$

where  $\sigma$  is the standard deviation of the surface heights,  $\eta$  is the areal asperity density, and  $R$  is the asperity radius.

GW [1] also define a plasticity index from these surface properties and the critical interference, which is given as

$$\psi = \sqrt{\frac{\sigma_s}{\omega_c}}. \quad (12)$$

The plasticity index relates the critical interference and the roughness of the surface to the plastic deformation of the surface. A higher plasticity index indicates a surface whose asperities are more likely to yield. Asperities are thus more likely to deform plastically on rougher surfaces with lower critical interference values. GW [1] suggest that for real surfaces the plasticity index can range from  $\psi = 0.1$  to 100. In this work, this range will be analyzed by holding the surface properties constant and varying the material yield strength, which differs from previous approaches that usually vary the surface profile properties.

### 4. Limitations of the statistical model

The outlined statistical model is only valid when the individual asperity contact models are also valid. Most asperity contact models assume that the deformations are relatively small and limited to the asperity tip. When  $a/R = 0.41$  the deformations are quite massive, however the current results are not intended to be used past that point, because Jackson and Green [2] did not consider larger amounts of deformation. Thus, during calculation of the current results the integrations of Eqs. (A.8) and (A.9),  $a/R$  should remain smaller.

From Eq. (5), the radius of contact can be written as

$$a = \sqrt{D\omega R}, \quad (13)$$

where

$$\text{For } 0 \leq \omega/\omega_c \leq 1.9$$

$$D = 1.$$

$$\text{For } \omega \geq 1.9\omega_c$$

$$D = \left( \frac{\omega}{1.9\omega_c} \right)^B \quad (14)$$

and  $B$  is found from Eq. (7). Thus, the equation for  $a/R$  can be written as

$$\frac{a}{R} = \frac{\sqrt{D\omega R}}{R} = \frac{\sqrt{D\omega}}{\sqrt{R}} \tag{15}$$

The normalized interference ( $\omega^* = \omega / \sigma$ ) is then substituted into Eq. (15) yielding

$$\frac{a}{R} = \frac{\sqrt{D\omega^*\sigma}}{\sqrt{R}} \tag{16}$$

From this point forward, units of length will be normalized by  $\sigma$  and designated by a star superscript. This analysis uses a minimal value  $D = 1$ , reducing Eq. (13) to the Hertzian result given in Eq. (A.10). Also,  $\omega^* = 1$  is arbitrarily used because at this value a large number of the asperities on the rough surface are clearly in contact. These values are conservative in that for elasto-plastic contact  $D$  is larger than one, and  $\omega^*$  can sometimes be larger than one for heavily loaded contacts. Clearly, this is not a concern for lightly loaded contacts.

A sampling of the experimental values reported by Nuri and Halling [8] and implemented in numerical simulations by Chang et al. [9] and Zhao et al. [10], are presented in Table 1, along with the resulting values of  $\sigma/R$  and  $a/R$ , using  $D = 1$  and  $\omega^* = 1$ . The resulting values of  $a/R$  indicate that very large deformations are being modeled. Even for sample one, the contact radius is approximately 10% of the asperity radius ( $a/R = 0.097$ ). Assuming Nuri and Hallings' data is realistic, these results put into question the validity of the statistical model used by Chang et al. [9], Zhao et al. [10], and even originally by GW [1]. In reality, the values of  $a/R$  will be larger than those calculated in Table 1 because both  $D$  and  $\omega^*$  can assume values (sometimes significantly) larger than one. The values in Table 1 also suggest that many real rough surfaces may undergo extreme deformations during asperity contact and that the bulk material below the asperities would likewise deform significantly (a condition that is not considered in any of the existing single asperity contact models).

It is clearly evident, that great care should be taken when using the statistical model first used by GW [1], and all subsequent models. Otherwise, the models may be calculating the contact area and contact force for deformations outside of their intended range. These calculations could thus produce meaningless or misleading results. The  $R$  and  $\sigma$  values used in the current analysis produce acceptable values for  $a/R$ .

Table 1  
Experimental surface parameters [8]

Sample	$\sigma$ ( $\mu\text{m}$ )	$R$ ( $\mu\text{m}$ )	$\sigma/R$	$(a/R)^a$
1	0.16	16.81	0.00941	0.097
2	1.35	7.14	0.190	0.44
3	3.94	6.12	0.643	0.80

<sup>a</sup>Based on Eq. (16) and assuming  $D = 1$ , and  $\omega^* = 1$ .

## 5. Results and discussion

This analysis uses the surface and material properties corresponding to a very smooth surface (see Table 2). Such smooth surfaces are often seen in MEMS and between other polished surfaces. The plasticity index is varied over the range shown in Table 3 by varying the yield strength to the values also shown. This is different than most works in that the plasticity index is often varied by changing the standard deviation of the asperity heights,  $\sigma_s$ . Eqs. (A.8) and (A.9) are then solved using each of the asperity contact models outlined above for  $\bar{P}$  and  $\bar{A}$ . The integrals are numerically evaluated using 10-point Gauss–Legendre quadrature. This procedure is evaluated by comparing the numerical results to the analytical approximation of Green [11] in Fig. 2.

The numerically evaluated CEB model is compared to the analytical solution of the CEB model provided by Green [11] in Fig. 2. For each solution, the contact area ratio ( $A/A_n$ ) is plotted as a function of the dimensionless load ( $P/(EA_n)$ ). First, this plot verifies that the numerically evaluated integrals produce nearly identical results as Green's solution for large plasticity indices ( $\psi = 4.0$ ). Second, there is a significant amount of error between Green's solution and the numerical results at small plasticity indices ( $\psi = 0.5$ ). Thus, when the Hertz elastic solution is dominant, numerical techniques should be used to solve the CEB model (by definition this solution is identical to the GW model as shown in Fig. 2). Although when Eqs. (A.14) and (A.15) are dominant, Green's solution provides accurate values. This makes sense because Green solves exactly the elasto-plastic portion of the CEB model (Eqs. (A.14) and (A.15)) and only approximates the elastic portion (Eqs. (A.10) and (A.11)).

Fig. 3 shows the resulting contact area ratios ( $A/A_n$ ) versus the dimensionless load ( $P/(EA_n)$ ) for different plasticity indices. The upper range of dimensionless load ( $P/(EA_n)$ ) shown in the plots represents heavily cases and is not typically encountered in common applications. As expected, the contact area increases with the load (see

Table 2  
Material and surface properties implemented in analysis

$E = 200$ Gpa
$\nu = 0.32$
$R = 2.0$ $\mu\text{m}$
$\sigma = 9.0$ nm
$\eta = 100.0 \times 10^{11}$ m <sup>-2</sup>

Table 3  
Plasticity indices and corresponding yield strengths

$\psi^a$	0.5	1.0	2.0	10.0	40.0	70.0	100.0
$S_y$ (GPa)	11.6	5.79	2.89	0.579	0.145	0.0827	0.0579

<sup>a</sup>From Eq. (12),  $\omega_c^* = \sigma_s/(\psi^2\sigma)$ , and is used to relate  $\psi$  and  $S_y$ .

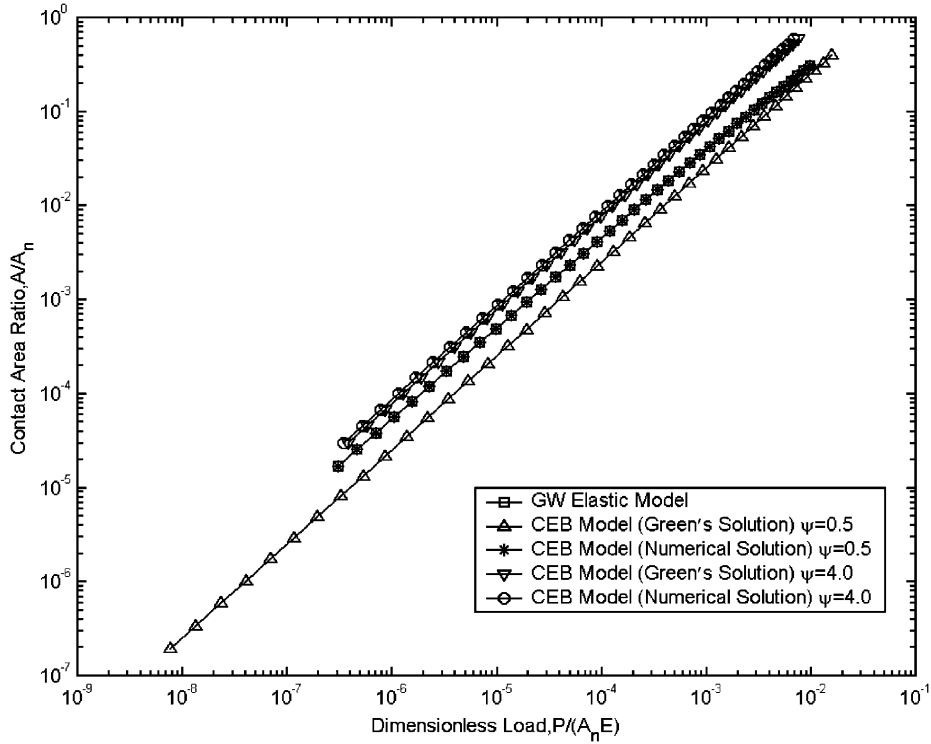


Fig. 2. Comparison of numerically and analytically produced results for the CEB model.

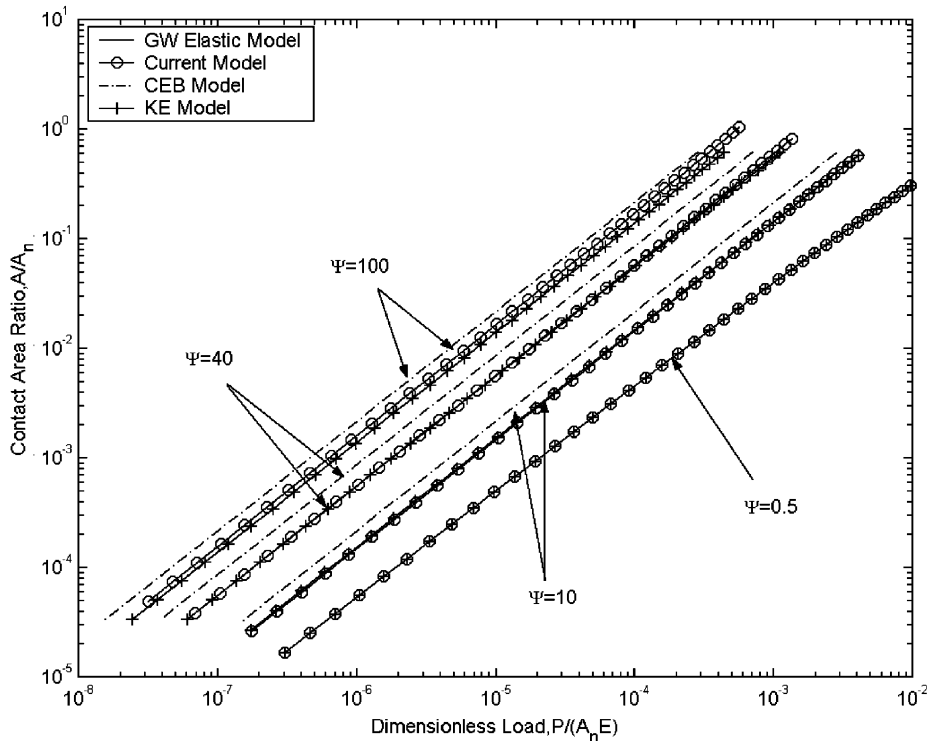


Fig. 3. Contact area versus load for various values of the plasticity index.

Fig. 1). The plot also indicates that an increase in the plasticity index results in larger contact areas at the same loads. When  $\psi = 0.5$ , all the models converge to the GW

model and are dominated by the Hertz elastic solution. As the plasticity index increases, so do the differences between the models. At  $\psi = 10$  the CEB differs from all other

models, while the KE and the current model still differ relatively little in comparison to each other. For higher plasticity indices the CEB model always has a larger

contact area than the other models. Once  $\psi = 40$  is reached, slight differences appear between the KE and the current model. At  $\psi = 40$  it appears that the lines

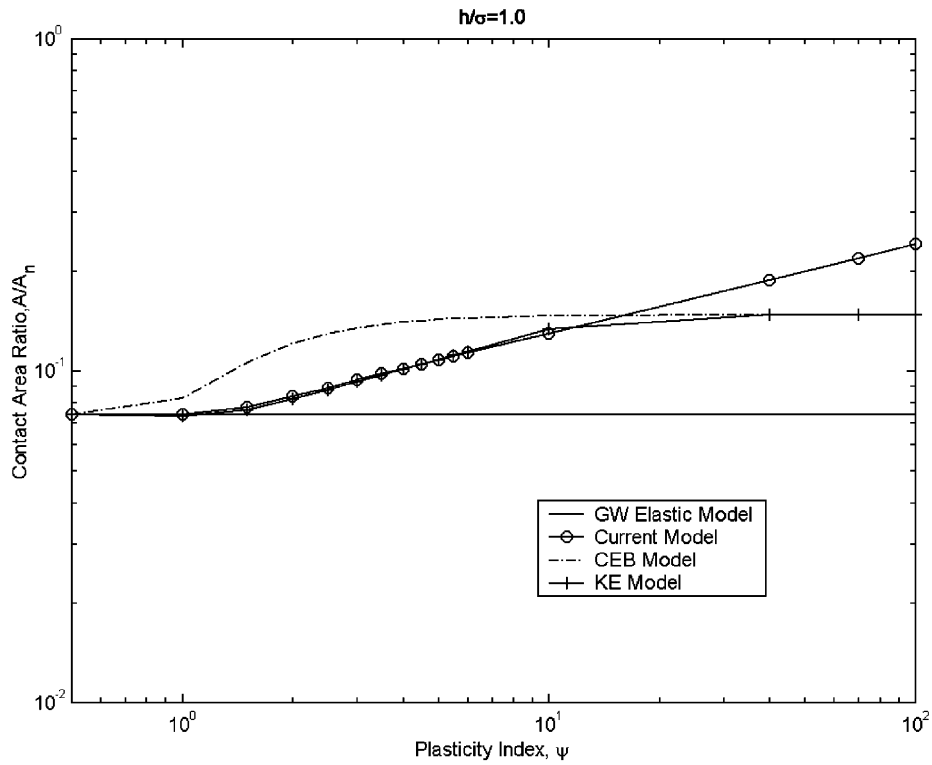


Fig. 4. Comparison of predicted contact areas.

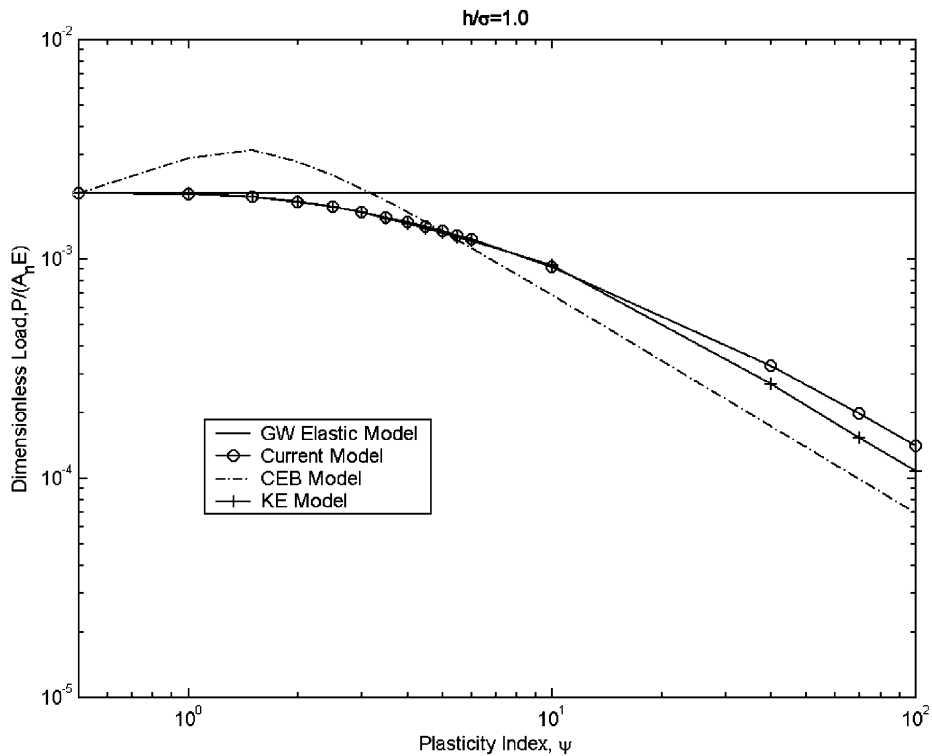


Fig. 5. Comparison of predicted contact loads.

predicted by the KE and the current model fall on top of each other. However, individual data points calculated from surface separation values (represented by the symbols) do not fall on top each other, indicating differences between the models. Finally, at  $\psi = 100$  it is clear that at the same load the contact area predicted by the current model is larger than the KE model. This is because the KE model's contact area is limited by the truncation model at large interferences (see Appendix A).

Next, the contact area ratio for each model is plotted as a function of the plasticity index, while  $h^*$  is held constant at a value of 1.0 (see Fig. 4). At low  $\psi$ , all the models follow the GW model, before any significant plastic deformation occurs. The CEB model clearly increases too quickly with  $\psi$ . The CEB predicts this because it assumes the volume conservation model (Eq. (A.14)), which overestimates contact area, immediately after  $\omega$  becomes greater than  $\omega_c$ . Once again, the KE and CEB models are clearly limited by assuming the truncation model at large plasticity indices. However, the current and KE model follow closely initially, but then the current model continues past both the CEB and KE models. As reported in Jackson and Green [2], the truncation model is invalid, and that is clearly evident in Fig. 4.

The dimensionless load is also plotted as a function of the plasticity index in Fig. 5. All the models again begin at the GW model when  $\psi = 0.5$ . However, the CEB immediately increases past the GW model. This is physically not possible since the GW model is elastic and is thus the limiting case. The CEB model predicts this because it assumes the volume conservation model (Eq. (A.15)) at  $\omega > \omega_c$ , and then also assumes that the contact area becomes fully plastic, thus overestimating contact area and load. Both the KE and the current model slowly decrease from the GW model as the plasticity index is increased. At  $\psi = 10$  the KE and current model differ by only 1.7%, but at  $\psi = 100$  this difference increases to 23%.

Overall though, and especially at plasticity indices less than ten, the two models agree fairly well due to an averaging effect of the integrals in Eqs. (A.8) and (A.9). Thus, even though the individual asperity contact results of the KE and current model differ quite appreciably at some interferences, the integration averages out these differences.

## 6. Conclusions

The KE model and the current model are found to be practically interchangeable at plasticity indices less than ten but have large differences at greater values. However, on a single asperity scale, it has been proven that the current model is a more complete model. This is especially true when the models are used to predict large deformations. The CEB model is also shown to be inaccurate since at some surface separations it predicts a higher load carrying capacity for surfaces deforming elasto-plastically than for those deforming only elastically (GW model). The contact area predicted by the KE and CEB models are also limited

by the truncation model, which the current work shows to incorrectly limit the contact area and the load.

It is also shown that the statistical models originally used by GW and subsequently used by Chang et al. [9], and Zhao et al. [10], among others, may not be valid for certain sets of surface parameters as indicated by Eq. (16). Great care should thus be taken when implementing Eqs. (A.8) and (A.9) for surfaces having large value for  $\sigma/R$ . This also suggests that the contact of rough surfaces will likely result in a large number of plastically deforming asperities.

## Appendix A. Summary of contact models

As mentioned in the main text, GW [1] show that rough surfaces can be modeled as a collection of individual asperities of various heights. These asperities are then categorized by a few statistical parameters describing the surface. First, the GW model assumes that all asperities have the same radius of curvature,  $R$ . Then, the distance between the surfaces can be described in two ways: (1) the distance between the mean of the surface heights,  $h$ , and (2) the distance between the mean of the summit heights or asperity peaks,  $d$ . These values are related by

$$h = d + y_s. \quad (\text{A.1})$$

The value of  $y_s$  is derived by Front [13] and given as

$$y_s = \frac{0.045944}{\eta R}, \quad (\text{A.2})$$

where  $\eta$  is the area density of the asperities.

When the surfaces are pressed together, some of the asperities will interfere a distance  $\omega$  with the opposing surface (see Fig. 1). Since the surfaces cannot penetrate each other,  $\omega$  is also the distance each asperity compresses perpendicular to the surfaces. The interference is defined as

$$\omega = z - d, \quad (\text{A.3})$$

where the height of each asperity is defined by a distance,  $z$ , from the mean asperity height. The heights of the asperities are also assumed to have a statistical distribution function,  $\phi(z)$ . In the current work the uncompromised Gaussian distribution is used, and the integrals are evaluated numerically. Although some past works have used a simplified exponential version of the Gaussian distribution (see [1,14,15–18]).

The nominal contact area,  $A_n$ , is the area of the surface upon which the asperities in contact are scattered. Thus, the number of asperities on the contacting surface can be found by multiplying the nominal surface area by the area density of the asperities:

$$N = \eta A_n. \quad (\text{A.4})$$

Then, the total number of asperities in contact is defined as

$$N_c = \eta A_n \int_d^\infty \phi(z) dz. \quad (\text{A.5})$$

The individual asperity contact area,  $\bar{A}$ , and force,  $\bar{P}$ , are functions of each asperity's interference,  $\omega$ . Thus, the contribution of all asperities of a height  $z$  to the total contact area and total contact force can be calculated as

$$A'(z) = \eta A_n \bar{A}(z - d) \phi(z), \quad (\text{A.6})$$

$$P'(z) = \eta A_n \bar{P}(z - d) \phi(z). \quad (\text{A.7})$$

Then, the total area of contact and total contact force between the surfaces is found by simply integrating Eqs. (A.6) and (A.7) over the entire range of asperity contact:

$$A(d) = \eta A_n \int_d^\infty \bar{A}(z - d) \phi(z) dz, \quad (\text{A.8})$$

$$P(d) = \eta A_n \int_d^\infty \bar{P}(z - d) \phi(z) dz. \quad (\text{A.9})$$

The GW model then assumes that the hemispherical asperities deform elastically and are defined by the Hertz elastic solution [19]. Detailed descriptions of the Hertz elastic solution are found in many common mechanics and tribology texts. The resulting equations for contact radius and force from the Hertz solution are

$$\bar{A}_E = \pi R \omega, \quad (\text{A.10})$$

$$\bar{P}_E = \frac{4}{3} E' \sqrt{R} (\omega)^{3/2}, \quad (\text{A.11})$$

where

$$\frac{1}{E'} = \frac{1 - \nu_1^2}{E_1} + \frac{1 - \nu_2^2}{E_2}, \quad (\text{A.12})$$

$$\frac{1}{R} = \frac{1}{R_1} + \frac{1}{R_2} \quad (\text{A.13})$$

and  $E_1, \nu_1, R_1, E_2, \nu_2, R_2$ , are the elastic properties and radii of sphere 1 and 2, respectively.

Instead of the Hertzian elastic solution, models which account for elasto-plastic deformation of an asperity can be used in Eqs. (A.8) and (A.9). A representation of these elasto-plastic models is outlined below. Because eventually any contact model accumulates statistically the contribution of all asperity contact points, the integration process tends to diminish the deviations between the various models (suggesting dominance by the statistics rather than by the models).

Chang et al. [9] developed a plastic contact model (CEB) that supplemented the GW [1] elastic contact model. First, the CEB model approximated elasto-plastic contact by modeling a plastically deformed portion of a hemisphere using volume conservation. The CEB model assumptions are discussed above, namely: (1) that the hemisphere deformation is localized to near its tip, (2) the hemisphere behaves elastically below the critical interference,  $\omega_c$ , and fully plastically above that value, and (3) the volume of the plastically deformed hemisphere is conserved. Using these assumptions the following approximations for contact area and force in the elastic-plastic range ( $\omega/\omega_c > 1$ ) are

analytically derived as

$$\bar{A}_{\text{CEB}} = \pi R \omega (2 - \omega_c/\omega) = \pi R (2\omega - \omega_c), \quad (\text{A.14})$$

$$\bar{P}_{\text{CEB}} = \pi R \omega (2 - \omega_c/\omega) K H = \pi R (2\omega - \omega_c) K H, \quad (\text{A.15})$$

where  $K$  is the hardness factor given by  $K = 0.454 + 0.41\nu$ . Also, the critical interference used in the CEB model, formulated somewhat differently than Eq. (1), is given by

$$\omega_c = \left( \frac{\pi K H}{2 E'} \right)^2 R, \quad (\text{A.16})$$

where the hardness is assumed to be  $H = 2.8 S_y$ . From an engineering perspective the corresponding values given by Eqs. (1) and (A.16) are very close. However, the CEB model is limited to this fixed relationship between the hardness and the yield strength, and the model also contains a discontinuity at  $\omega_c$ .

If the plastic deformation covers the entire area of contact, it is said that a fully plastic condition is reached. The fully plastic truncation model states that under fully plastic conditions the area of contact of an asperity pressed against a rigid flat can be approximately calculated by truncating the asperity tips as the rigid flat translates an interference,  $\omega$ . For a hemisphere, this approximated fully plastic area is given by

$$\bar{A}_p = 2\pi R \omega, \quad (\text{A.17})$$

which predicts larger contact areas than Eq. (A.10). Using Eq. (A.17), the contact force of the hemispherical asperity is simply the contact area multiplied by the average contact pressure, which in this case is the hardness, since the contact is assumed to be fully plastic. The fully plastic contact force is thus

$$\bar{P}_p = 2\pi R \omega H. \quad (\text{A.18})$$

Since plastic deformation of the asperity will increase the area of contact (see Fig. 1), the truncation model produces the proper trend to some degree. However, FEM results [2] show that this model is unjustifiable, since the contact area can become larger than that predicted by Eq. (A.17). Although this model is often attributed to Abbott and Firestone [12], they intended their model to be used to describe a wear process rather than an indentation process. Also, Greenwood and Tripp developed a similar model [20]. Throughout this work the Abbott and Firestone [12] model is referred to as the Truncation model.

KE [4] also performed an FEM analysis of the same case of an elastic-perfectly plastic sphere in contact with a rigid flat. Their work gives a very detailed analysis of the stress distribution in the contact region, and empirical expressions are provided for the contact area and the contact force. These are given in a piece-wise form:

$$\text{For } 1 \leq \omega/\omega_c \leq 6$$

$$\bar{P}_{\text{KE}} = \bar{P}_c 1.03 \omega/\omega_c^{1.425}, \quad (\text{A.19})$$

$$\bar{A}_{\text{KE}} = \bar{A}_c 0.93 \omega/\omega_c^{1.136}. \quad (\text{A.20})$$

For  $6 \leq \omega/\omega_c \leq 110$

$$\bar{P}_{KE} = \bar{P}_c 1.40 \omega / \omega_c^{1.263}, \quad (\text{A.21})$$

$$\bar{A}_{KE} = \bar{A}_c 0.94 \omega / \omega_c^{1.146}. \quad (\text{A.22})$$

These equations are discontinuous at  $\omega/\omega_c = 1$  and 6, and they describe the deformation only up to  $\omega/\omega_c = 110$ , at which point the fully plastic Truncation model is assumed [4,21]. The KE model also assumes the value of  $H$  to be fixed at  $2.8S_y$ . KE [21] also use the above single asperity model in a numerical statistical model similar to the one presented in this work. All aforementioned models apply to static conditions.

## References

- [1] Greenwood JA, Williamson JBP. Contact of nominally flat surfaces. Proc R Soc Lond A 1966;295:300–19.
- [2] Jackson RL, Green I. A finite element study of elasto-plastic hemispherical contact. ASME J Tribol 2005;127:343–54.
- [3] Mesarovic SD, Fleck NA. Frictionless indentation of dissimilar elastic–plastic spheres. Int J Solids Struct 2000;37:7071–91.
- [4] Kogut L, Etsion I. Elastic–plastic contact analysis of a sphere and a rigid flat. J Appl Mech Trans ASME 2002;69(5):657–62.
- [5] Tabor D. The hardness of materials. Oxford: Clarendon Press; 1951.
- [6] Quicksall J, Jackson RL, Green I. Elasto-plastic hemispherical contact for varying mechanical properties. IMechE J Eng Trib—Part J 2004;218:313–22.
- [7] McCool JI. Comparison of models for the contact of rough surfaces. Wear 1986;107:37–60.
- [8] Nuri KA, Halling J. The normal approach between rough flat surfaces in contact. Wear 1975;32:81–93.
- [9] Chang WR, Etsion I, Bogy DB. An elastic–plastic model for the contact of rough surfaces. ASME J Tribol 1987;109:257–63.
- [10] Zhao Y, Maletta DM, Chang L. An asperity microcontact model incorporating the transition from elastic deformation to fully plastic flow. ASME J Tribol 2000;122:86–93.
- [11] Green I. A transient dynamic analysis of mechanical seals including asperity contact and face deformation. Trib Trans 2002; 45(3):284–93.
- [12] Abbott EJ, Firestone FA. Specifying surface quality—a method based on accurate measurement and comparison. Mech Eng 1933; 55:569–72.
- [13] Front I. The effects of closing force and surface roughness on leakage in radial face seals. MS thesis, Technion, Israel Institute of Technology, 1990.
- [14] Etsion I, Front I. Model for static sealing performances of end face seals. Trib Trans 1994;37(1):111–9.
- [15] Polycarpou AA, Etsion I. Analytical approximations in modeling contacting rough surfaces. ASME J Tribol 1999;121(2):234–9.
- [16] Hess DP, Soom A. Normal and angular motions at rough planar contacts during sliding with friction. ASME J Tribol 1992;114(3): 567–78.
- [17] Hess DP, Soom A. Effects of relative angular motions on friction at rough planar contacts. ASME J Tribol 1993;115(3):96–101.
- [18] Liu Z, Neville A, Reuben RL. Analytical solution for elastic and elastic–plastic contact models. Trib Trans 2000;43(4):627–34.
- [19] Timoshenko S, Goodier JN. Theory of elasticity. New York: McGraw-Hill; 1951.
- [20] Greenwood JA, Tripp JH. The contact of two Nominally flat rough surfaces. Proc Inst Mech Eng 1971;185:625–33.
- [21] Kogut L, Etsion I. A finite element based elastic–plastic model for the contact of rough surfaces. Tribol Trans 2003;46:383–90.